Computer Assisted Mechanics and Engineering Sciences, **12**: 31–48, 2005.

Nonlinear dynamic dnalysis of high speed rolling element bearings due to cage run-out

S. P. Harsha, P. K. Kankar,
Mechanical Engineering Group, Birla Institute of Technology & Science, Pilani-333031 (India); Phone No:. +91-01596-242210; Fax No.: +91-01596-244183

R. K. Purohit
Member of ASME, M. B. M. Engineering College, J. N. V. U. - Jodhpur (India)

(Received October 23, 2003)

The paper presents an analytical model to investigate the nonlinear dynamic behavior of rotor bearing system due to cage run-out. Due to run-out of the cage, the rolling elements no longer stay equally spaced. The mathematical model takes into account the sources of nonlinearity such as Hertzian contact force and cage run-out, resulting transition from no contact-to-contact state between rolling elements and races. The contact between the rolling elements and races is treated as nonlinear springs. The nonlinear stiffness is obtained by application of Hertzian contact deformation theory. The implicit type numerical integration technique Newmark-β with Newton Raphson method is used to solve the nonlinear differential equations iteratively. The results are presented in the form of Fast Fourier Transformations (FFT) and contact force-time responses. It is implied from the obtained FFT that due to the cage run-out, the ball passage frequency is modulated with the cage frequency.

Keywords: nonlinear dynamic response, chaotic vibration, Newmark-β, ball passage frequency

NOTATIONS

c	equivalent viscous damping factor, Ns/m,
f_{eq}	equivalent frequency of damping force, s^{-1},
$F_{\theta i}$	local Hertzian contact force, N,
F_u	force due to unbalance rotor, N,
k	constant for Hertzian contact elastic deformation, $\text{N/m}^{3/2}$,
N_b	number of balls,
r	inner race radius, mm,
R	outer race radius, mm,
$r_{\theta i}$	displacement at i^{th} ball, μm,
t	time, sec,
V_{cage}	translational velocity of the cage center, mm/s,
V_{inner}	translational velocity of the inner race, mm/s,
V_{outer}	translational velocity of the outer race, mm/s,
W	radial load, N,
x, y	axial displacements, μm,
Γ	cage run-out, μm,

ω_{bp} ball Passage speed, rad/s,
ω_{cage} angular speed of the cage, rad/s,
ω_{inner} angular speed of the inner race, rad/s,
ω_{rotor} angular speed of the rotor, rad/s,
ω_{outer} angular speed of the outer race, rad/s,
ω_{wp} wave Passage speed, rad/s,
θ_i angular location of i^{th} rolling element, rad,
BPF Ball Passage Frequency,
FFT Fast Fourier Transformations.

1. Introduction

Rolling element bearings are a non-negligible source of vibration in many types of rotating machine. The behavior of nonlinear systems often demonstrates unexpected behavior patterns that are extremely sensitive to initial conditions. Many advanced bearing applications now require understanding of dynamic effects and classical quasi-static analysis techniques of Jones [1], Harris [19], Palmgren [2] and others are inadequate for dynamic analysis. Cage failures due to high pocket wear or destructive collision forces between the cage and rolling element or race lands, cage induced audio noise, structural vibration and excessive torque or torque noise, which are the examples of bearing performance characteristics that are significantly affected by cage dynamics. Rolling element to cage interactions can induce excessive vibrations then ball to race skidding and degraded performance. This can cause premature failure in the system. When ball bearings are operated at high speed, they generate vibrations and noise. The principle forces, which drive these vibrations, are time varying nonlinear contact forces, which exist between the various components of the rotor bearing system: balls, races and rotor.

Since today, ball bearings are used in the design of increasingly sophisticated arrangements, involving high speed, high temperature, heavy or unusual loading and requiring continuous operations, automation etc., a clear understanding of vibrations associated with them is needed. It is generally accepted that it is impossible to produce a perfect surface or contour even with the best machine tools and this applies also in ball bearing manufacturing. In the rotor bearing assembly supported by perfect ball bearings, the vibrations at the natural frequency and the varying compliance frequency dominate the vibration spectrum. The vibrations at this later frequency are called varying compliance vibrations.

Walters [6] developed an analytical model for ball bearing and cage dynamics with ball raceway slip that was later modified by Gupta [14, 15]. However, the solution of time varying Hertzian contact stress for each ball, along with integration of each cage impact with the balls or raceways and integration of the ball traction/slip forces at each contact point on the inside and outside raceways, results in the long computer run times and can be so costly as to make parametric design studies impractical. In addition, the Walters/Gupta model equations are written in fixed inertial coordinate system which leads to complex equations of motion, excessively long computer times and computational errors due to computer numerical truncation. Kennel and Bupara [10] developed a simplified method for analyzing ball and cage dynamics and assumed that the ball cage is only to move in the plane of its major diameter. Meeks et al. [3, 4] have shown that the ball cage motions are far too complex to be modeled with this extreme simplification of cage motion. Meeks [5] developed an analytical model to study and optimize the bearing and cage design parameters. Gad et al. [7] showed that resonance occurs when the ball passage frequency (BPF) coincides with a natural frequency of the system and they also pointed out that for certain speeds, BPF can exhibit its sub and super harmonic vibrations for shaft ball bearing system. Rahnejat and Gohar [9] showed that even in the presence of an elasto-hydrodynamic lubricating film between balls and the races, a peak at the BPF appears in the spectrum. Aktürk et al. [12] performed a theoretical investigations

of effect of varying the preload on the vibration characteristics of a shaft bearing system and also suggested that by taking the correct number of balls and amount of preload in a bearing untoward effect of the BPF can be reduced.

Harsha et al. [16] developed an analytical model to predict nonlinear dynamic response in a rotor bearing system due to surface waviness. The conclusion of this work shows that for the *outer race waviness*, the severe vibrations occur when the number of balls and waves are equal. In case of the *inner race waviness*, the peak amplitude of vibration can be at $q\omega_{\text{wp}} \pm p\omega_{\text{cage}}$. For the waviness order iN_b, peak amplitude of vibration and super-harmonic appear at the wave passage speed (ω_{wp}). Harsha et al. [17] analyzed the nonlinear behaviors of ball bearing due to number of balls and preload effect. Nonlinear dynamic response is found to be associated with the ball passage frequency. The amplitude of the vibration is considerably reduced if the number of balls and preload are correctly selected. Harsha et al. [18] analyzed the nonlinear behaviors of the high-speed horizontal balanced rotor supported by ball bearings. The conclusion of this work shows that most severe vibrations occur when the ball passage frequency (BPF) and its harmonics coincide with the natural frequency.

In this paper, a theoretical investigation was conducted to observe the effect of cage run-out on the vibration characteristics of ball bearing system. The system is considered with the assumption that there is no friction between the rolling elements and races. In terms of the feature that the nonlinear bearing forces act on the system, the implicit type numerical integration technique Newmark-β [11] with Newton Raphson method is used to solve the nonlinear differential equations iteratively. The results obtained from a large number of numerical integrations are mainly presented in form of Fast Fourier Transformation (FFT) and contact force-time response.

2. Modeling of the system

To analyze the structural vibrations in rolling element bearings a model is developed in which the outer race of the bearing is fixed in a rigid support and the inner race is fixed rigidly with the shaft. A constant radial vertical force acts on the bearing. Elastic deformation between race and ball gives a nonlinear force-deformation relation, which is obtained by using the Hertzian theory. Other sources of stiffness variation are the cage run-out, the finite number of balls whose position change periodically and waviness at the inner and outer race, all of them cause periodic changes in stiffness of the bearing assembly. The governing differential equations are obtained by taking into account these sources of stiffness variation.

A schematic diagram of a rolling element bearing is shown in Fig. 1. In the mathematical model, the rolling element bearings are considered as a mass-spring system and the contact acts as a nonlinear contact spring. The Hertzian forces arise only when there is contact deformation, the springs are required to act only in compression. In other words, the respective spring force appears when the instantaneous spring length is shorter than its unstressed length, otherwise the separation between ball and race takes place and the resulting force is set to zero. The assumptions made in development of the mathematical model are as follows:

1. The outer race is fixed rigidly to the support and the inner race is fixed rigidly to the shaft.
2. The rolling element, the inner and outer races and the cage have motions in the plane of the bearing only. This eliminates any motion in the axial direction.
3. The bearings are assumed to operate under isothermal condition.
4. Deformations occur according to the Hertzian theory of elasticity. Hence, only small elastic motions of the rolling elements and the rings are considered.
5. The cage ensures the constant angular separation (β) between rolling elements, hence there is no interaction between rolling elements. Therefore,

$$\beta = \frac{2\pi}{N_b}. \tag{1}$$

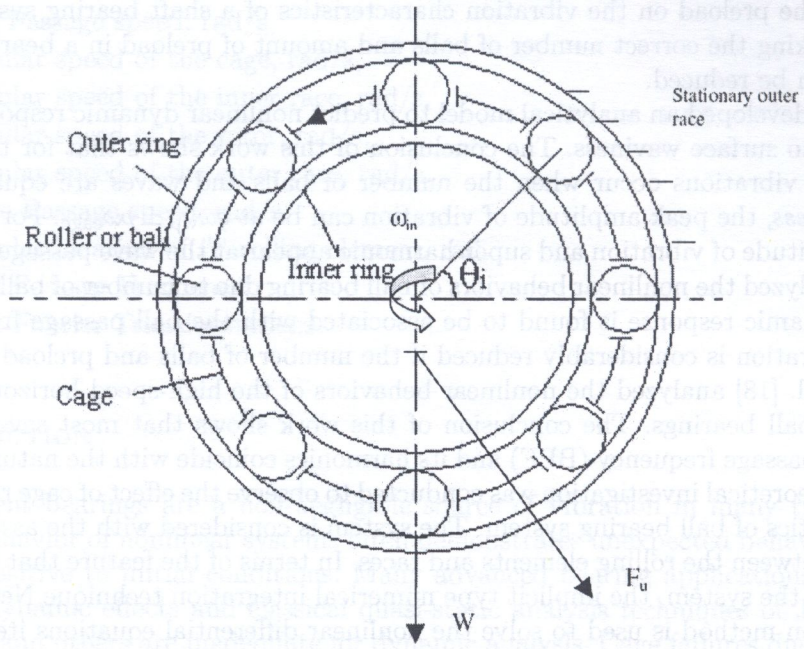

Fig. 1. A schematic diagram of a rolling element bearing

There is no slipping of balls as they roll on the surface of races. Since there is perfect rolling of the balls on the surface of races and the two points of ball touching the races have different linear velocities, the center of the ball has a resultant translational velocity. The translational velocity of the center is,

$$V_{\text{cage}} = \frac{V_{\text{inner}} + V_{\text{outer}}}{2}, \tag{2}$$

where,

$$V_{\text{outer}} = \omega_{\text{outer}} \times R, \tag{3}$$

$$V_{\text{inner}} = \omega_{\text{inner}} \times r. \tag{4}$$

Here the outer race is assumed to be stationary, $V_{\text{outer}} = 0$. Therefore

$$V_{\text{cage}} = \frac{V_{\text{inner}}}{2} = \frac{\omega_{\text{inner}} \times r}{2}. \tag{5}$$

Now the angular velocity of the cage (ω_{cage}) about the center of inner race is,

$$\omega_{\text{cage}} = \frac{V_{\text{cage}}}{(R+r)/2} = \frac{\omega_{\text{inner}} \times r}{(R+r)}. \tag{6}$$

Since inner race is rigidly fixed to the rotor, hence $\omega_{\text{inner}} = \omega_{\text{rotor}}$. Therefore

$$\omega_{\text{cage}} = \omega_{\text{rotor}} \left(\frac{r}{r+R}\right). \tag{7}$$

The ball passage frequency is:

$$\omega_{\text{bp}} = \omega_{\text{cage}} \times N_b. \tag{8}$$

6. The damping of a ball bearing is very small. The damping occurs because of friction and small amount of lubrication. The estimation of damping in ball bearing is very difficult because of the dominant extraneous damping which swamps the damping of the bearing. Kramer [8] has provided an estimation of the bearing damping. The element race vibratory system is reduced to a linear spring mass damper system for which ω_{eq}, the frequency at which the amplitude of the damping force equals the spring force when a harmonic motion is given to the system, is evaluated. From literature, Kramer [8], we have,

$$f_{eq} = \frac{\omega_{eq}}{2\pi} = (0 \text{ to } 4)\ 10^5 \quad \text{s}^{-1}, \tag{9}$$

$$c = (0.25 \text{ to } 2.5)\ 10^{-5} k \quad (\text{Ns}/\mu\text{m}), \tag{10}$$

where k is the linearized stiffness of the ball bearing.

2.1. Cage run-out

Due to the run-out of the cage, the rolling elements no longer stay equally spaced, as shown in Fig. 2.

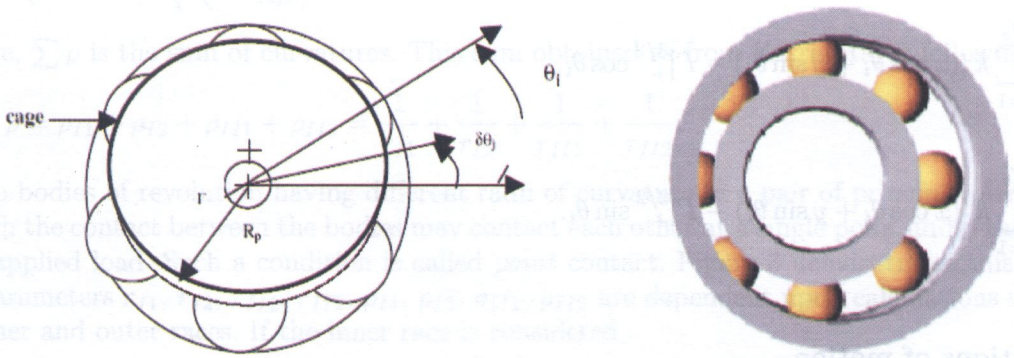

Fig. 2. Non-uniform ball spacing due to cage run-out

The resulting variations of the circumferential angle for a small run-out Γ is:

$$\delta\theta_i = \frac{\Gamma}{R_p} \cos(\theta_i), \tag{11}$$

where R_p denotes the pitch radius.

Due to the non-uniform spacing, the varying compliance frequency is modulated with the cage frequency. The angular excitation frequencies due to the cage run-out are given by

$$\omega = a\omega_{bp} \pm b\omega_{cage} = a\, N_b \omega_{cage} \pm b\omega_{cage}, \tag{12}$$

where a and b are the constants.

2.2. Calculation of the restoring force

The local Hertzian contact force and deflection relationship for the bearing may be written as:

$$F_{\theta_i} = k\,(r_{\theta_i})^{3/2}. \tag{13}$$

Performing the elastic analysis of Hertzian contact between the inner race, the outer race and the ball, the value of $k$can be obtained.

The radial displacement $(r\theta_i)$ at the i^{th} ball is given as:

$$r_{\theta_i} = x\cos\theta_i + y\sin\theta_i. \tag{14}$$

Considering the cage run-out, the contact deformation becomes,

$$r_{\theta_i} = x\cos\theta_i + y\sin\theta_i - (\Gamma)\,. \tag{15}$$

Substituting r_{θ_i}in the Eq. (13), we get

$$F_{\theta_i} = k\left[(x\cos\theta_i + y\sin\theta_i) - \Gamma\right]_+^{3/2}. \tag{16}$$

If the expression inside the bracket is greater than zero, then the ball at the angular location θ_i is loaded giving rise to a restoring force F_{θ_i}. If the expression in the bracket is negative or zero, then the ball is not in the load zone, and the restoring force F_{θ_i} is set to zero. The total restoring force is the sum of restoring force from each of the rolling elements. Thus the total restoring force components in the X and Y directions are,

$$F_x = \sum_{i=1}^{N_b} k\left[(x\cos\theta_i + y\sin\theta_i) - \Gamma\right]_+^{3/2}\cos\theta_i, \tag{17a}$$

$$F_y = \sum_{i=1}^{N_b} k\left[(x\cos\theta_i + y\sin\theta_i) - \Gamma\right]_+^{3/2}\sin\theta_i. \tag{17b}$$

2.3. Equations of motion

The system governing equations accounting for inertia, restoring and damping force and constant vertical force acting on the inner race are,

$$m\ddot{x} + c\dot{x} + \sum_{i=1}^{N_b} k\left[(x\cos\theta_i + y\sin\theta_i) - \Gamma\right]_+^{3/2}\cos\theta_i = W + F_u\cos(\omega t)\,, \tag{18a}$$

$$m\ddot{y} + c\dot{y} + \sum_{i=1}^{N_b} k\left[(x\cos\theta_i + y\sin\theta_i) - \Gamma\right]_+^{3/2}\sin\theta_i = F_u\sin(\omega t)\,. \tag{18b}$$

Here, m is the mass of the rotor supported by bearings. The system Eq. (18) is two coupled non-linear ordinary second order differential equations having parametric effect, the 1.5 nonlinearity and the summation term. The '+' sign as subscript in these equations signifies that if the expression inside the bracket is greater than zero, then the rolling element at angular location θ_i is loaded giving rise to restoring force and if the expression inside bracket is negative or zero, then the rolling element is not in the load zone, and restoring force is set to zero. The damping in this system is represented by an equivalent viscous damping c. The value of damping coefficient has been estimated using Eq. (10). The unbalance force F_u is taken for balanced rotor as zero.

2.4. Contact stiffness

The Hertz equations for elastic deformation involving *point* contact between solid bodies are given by Eschmann [13] as:

$$r_{\theta_i} = 1.5\frac{2K}{\Lambda\mu}\sqrt[3]{\frac{\left(1-\frac{1}{M}\right)^2 \sum\rho}{3E^3}Q^2}. \tag{19}$$

Here, Λ, K and μ are Hertz coefficients which depend on the surface properties. E, $1/M$ and $\sum\rho$ are the elastic modulus in $\mathrm{N/mm^2}$, Poisson ratio and the sum of curvature of the contacting bodies, respectively. The contact force Q is:

$$Q = \frac{E}{\left(1-\frac{1}{M^2}\right)}\sqrt{\frac{3r_{\theta_i}}{\left(1.5\frac{2K}{\Lambda\mu}\right)^3 \sum\rho}}\, r_{\theta_i}. \tag{20}$$

Hence the nonlinear stiffness associated with point contact is:

$$k = \frac{E}{\left(1-\frac{1}{M^2}\right)}\sqrt{\frac{3r_{\theta_i}}{\left(1.5\frac{2K}{\Lambda\mu}\right)^3 \sum\rho}}. \tag{21}$$

Here, $\sum\rho$ is the sum of curvatures. This sum obtained as from Harris [19] is following:

$$\sum\rho = \rho_{I1} + \rho_{I2} + \rho_{II1} + \rho_{II2} = \frac{1}{r_{I1}} + \frac{1}{r_{I2}} + \frac{1}{r_{II1}} + \frac{1}{r_{II2}}. \tag{22}$$

Two bodies of revolution having different radii of curvature in a pair of principle planes passing through the contact between the bodies may contact each other at a single point under the condition of no applied load. Such a condition is called *point* contact. Figure 3 demonstrates this condition. The parameters r_{I1}, r_{I2}, r_{II1}, r_{II2}, ρ_{I1}, ρ_{I2}, ρ_{II1}, ρ_{II2} are dependent upon calculations referring to the inner and outer races. If the inner race is considered,

$$\begin{aligned} &r_{I1} = D/2, \quad r_{I2} = D/2, \quad r_{II1} = r, \quad r_{II2} = r \quad \text{and} \\ &\rho_{I1} = 2/D, \quad \rho_{I2} = 2/D, \quad \rho_{II1} = 1/r, \quad \rho_{II2} = -1/r. \end{aligned} \tag{23}$$

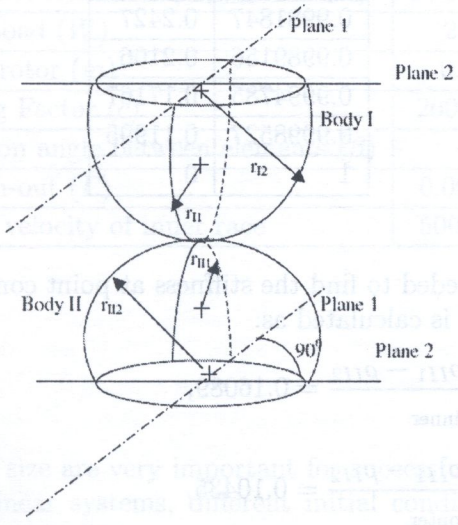

Fig. 3. Geometry of contacting bodies

If the outer race is considered, the parameters are:

$$r_{I1} = D/2, \quad r_{I2} = D/2, \quad r_{II1} = R, \quad r_{II2} = R \quad \text{and}$$
$$\rho_{I1} = 2/D, \quad \rho_{I2} = 2/D, \quad \rho_{II1} = -1/R, \quad \rho_{II2} = -1/R. \tag{24}$$

With the use of Table 1, the parameters are:

$$\text{For inner race } \rho_{I1} = \rho_{I2} = 0.41999, \quad \rho_{II1} = 0.21346, \quad \rho_{II2} = 0.0533674 \ (\text{mm})^{-1}$$
$$\text{For outer race } \rho_{I1} = \rho_{I2} = 0.41999, \quad \rho_{II1} = 0.141532, \quad \rho_{II2} = 0.0353832 \ (\text{mm})^{-1} \tag{25}$$

Table 1. Dimensional contact parameters from Ref. [19]:

$F(\rho)$	δ^*
0	1
0.1075	0.997
0.3204	0.9761
0.4795	0.9429
0.5916	0.9077
0.6716	0.8733
0.7332	0.8394
0.7948	0.7961
0.83595	0.7602
0.87366	0.7169
0.90999	0.6636
0.93657	0.6112
0.95738	0.5551
0.97290	0.4960
0.983797	0.4352
0.990902	0.3745
0.995112	0.3176
0.997300	0.2705
0.9981847	0.2427
0.9989156	0.2106
0.9994785	0.17167
0.9998527	0.11995
1	0

The value of $(2K/A\mu)$ is needed to find the stiffness at point contact from Eq. (21). To find out this value from the table, $\cos\tau$ is calculated as:

$$(\cos\tau)_{\text{inner}} = \frac{\rho_{I1} - \rho_{I2} + \rho_{II1} - \rho_{II2}}{(\sum\rho)_{\text{inner}}} = 0.16089,$$
$$(\cos\tau)_{\text{outer}} = \frac{\rho_{I1} - \rho_{I2} + \rho_{II1} - \rho_{II2}}{(\sum\rho)_{\text{outer}}} = 0.10435. \tag{26}$$

From the table given in Eschmann [13],

$\frac{2K}{A\mu} = 0.995$ (For both the inner and outer races.)

Hence, for both the inner and outer races the contact stiffness is the same.

Here we consider steel ball and steel raceway contacts, the elastic modulus and Poisson's ratio are as:

$$E = 2.0 \times 10^{11} \quad \frac{\mathrm{N}}{\mathrm{mm}^2} \quad \text{and} \qquad 1/M = 0.3 \tag{27}$$

Hence the Eq. (21) becomes

$$k = \frac{2 \times 10^5}{1 - (0.3)^2} \sqrt{\frac{3 r_{\theta_i}}{(1.5 \times 0.995)^3 \times 1.16089}} \quad \frac{\mathrm{N}}{\mathrm{mm}^{3/2}} \tag{28}$$

and thus:

$$k = 1.9845 \times 10^5 \sqrt{r_{\theta_i}} \quad \frac{\mathrm{N}}{\mathrm{mm}^{3/2}}. \tag{29}$$

3. Computational solution of the equations and results

The equations of motion (18) are solved using the modified Newmark-β method to obtain the radial displacement and velocity of the rolling elements. In order to eliminate the effect of the natural frequency an artificial damping was introduced into the system. With this damping, transient vibrations are eliminated. Thus, peak steady state amplitude of vibration can be measured. The longer the time to reach steady state vibrations, the longer CPU time needed and hence the more expensive the computation. A value of $c = 200$ Ns/m was chosen. To observe the nonlinear behavior of the system, parameters of the ball bearing are selected and are shown in Table 2.

Table 2. Geometrical properties of ball bearing

Ball Diameter (D)	4.762 mm
Inner Race Diameter (D_{inner} = r×2)	18.738 mm
Outer Race Diameter (D_{outer} = R×2)	28.262 mm
Radial Load (W)	2.4 N
Mass of rotor (m)	0.6 kg
Damping Factor (c)	200 Ns/m
Separation angle between elements (β)	45°
Cage run-out (Γ)	0.001 μm
Angular velocity of inner race	5000 rpm

3.1. Initial conditions

The initial conditions and step size are very important for successful and economic computational solution. Particularly for nonlinear systems, different initial conditions mean a totally different system and hence different solutions. The larger the time step Δt, the faster the computation. On

the other hand, the time step should be small enough to achieve an adequate accuracy. Also, very small time steps can increase the truncation errors. Therefore an optimization should be made between them. The time step for the investigation is assumed as $\Delta t = 10^{-5}$ sec. At time $t = 0$ the following assumptions are made:

i. The shaft is held at the center of the bearing and all balls are assumed to have equal axial preload.

ii. The shaft is then given initial displacements and velocities. For fast convergence the initial displacements are set to the following values: $x_0 = 10^{-6}$ m and $y_0 = 10^{-6}$ m. The initial velocities are assumed to be zero: $\dot{x} = 0$ and $\dot{y} = 0$.

iii. When $t \succ \Delta t$ the initial conditions have already passed and the normal procedure commences.

3.2. Cage run-out

The time history of the nonlinear responses has been examined for periodic behavior. This is done by examining the time series output, once per cycle, for sufficiently long segments of time step so that multiple periodic and aperiodic behaviors could be discerned from the post transient solutions. From force-time response, the system behavior can be observed. For a periodic response, a single point appears since the peak values of n cycles are same. For a sub-harmonic response, a few discrete points appear. For a chaotic response, a band of points appear since the peak force varies from one excitation to another and very large variations in peak contact force observed. Due to the cage run-out, the rolling elements no longer stay equally spaced. Due to the non-uniform spacing, the ball passage frequency is modulated with the cage frequency. The resulting variation of the circumferential angle for a small run-out Γ is assumed as 0.001 μm. The results of computations are presented in form of FFT and contact force time response.

Figure 4 shows the vibrations for the bearing with a cage run-out at different number of balls. When the number of balls is 4, the peak amplitude of vibration appears in the vibration spectrum at the frequency $\omega_{bp} + \omega_{cage} = 140$ Hz as shown in Fig. 4 (a). Other major peaks of vibration amplitude appear at an integral multiple of the ball passage with cage frequency $2\omega_{bp} + 2\omega_{cage} = 280$ Hz, $3\omega_{bp} + 3\omega_{cage} = 420$ Hz. In the force-time response few discrete points appear at the peak, which shows the 2–T periodic motion of the rolling element bearings. For 5 balls, the peak amplitude of vibration appears in the spectrum at the ball passage frequency $\omega_{bp} = 170$ Hz as shown in Fig. 4 (b). Other major peaks at super harmonics of vibration appear at an integral multiple of the ball passage frequency $2\omega_{bp} = 340$ Hz, $3\omega_{bp} = 510$ Hz, $2\omega_{bp} + 3\omega_{cage} = 442$ Hz. In the force-time response, few discrete points appear at the peak, which shows the 3–T periodic motion of the rolling element bearings. When the number of balls is 6, the peak amplitude of vibration appears in the spectrum at the ball passage frequency $\omega_{bp} = 204$ Hz as shown in Fig. 4(c).

Other major peaks at super harmonics of vibration appear at an integral multiple of the ball passage frequency $2\omega_{bp} = 408$ Hz, $3\omega_{bp} = 612$ Hz, $2\omega_{bp} + 2\omega_{cage} = 476$ Hz. In the force-time response, few discrete points appear at the peak, which shows the 3–T periodic motion of the rolling element bearings with less amplitude. For 7 balls, the peak amplitude appears at the ball passage frequency $\omega_{bp} = 238$ Hzas shown in Fig. 4 (d).

Other major peaks at super harmonics of vibration appear at an integral multiple of the ball passage frequency $2\omega_{bp} = 476$ Hz, $3\omega_{bp} = 714$ Hz, $2\omega_{bp} + \omega_{cage} = 510$ Hz. In the force-time response, few discrete points appear at the peak, which shows the 4–T periodic motion of the rolling element bearings. For 8 balls, the peak amplitude appears at $\omega_{bp} = 272$ Hz as shown in Fig. 4 (e). Other major peaks at super harmonics of vibration appear at $2\,\omega_{bp} = 544$ Hz. In the force-time response, few discrete points appear at the peak, which shows the 4–T periodic motion of the rolling element bearings with less amplitude. Similarly, for 9 to 17 balls, the peak amplitude of vibration appears in the spectrum at an integer multiple of the number of balls (N_b) and the cage speed (ω_{cage}) and

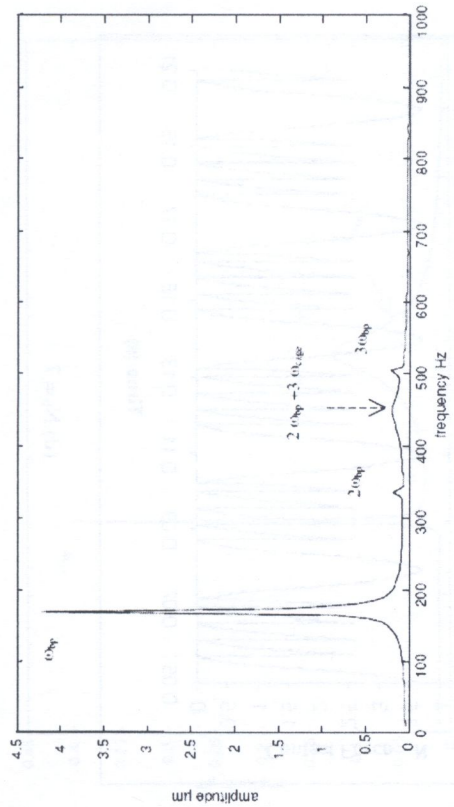
amplitude µm
frequency Hz

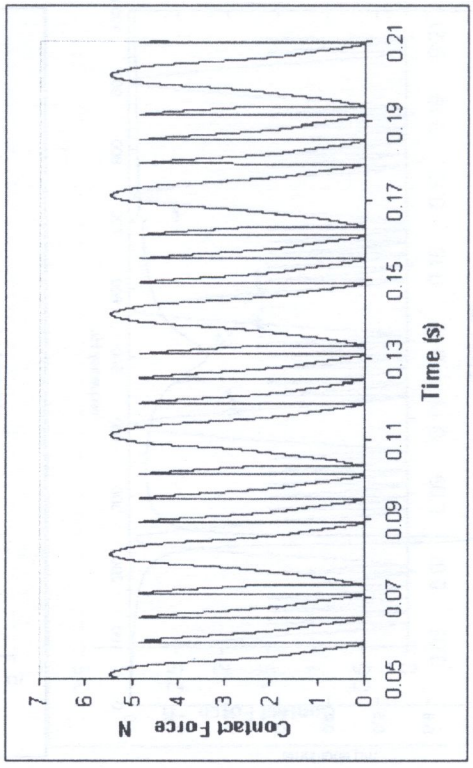
Contact Force N
Time (s)

(b) $N_b = 5$

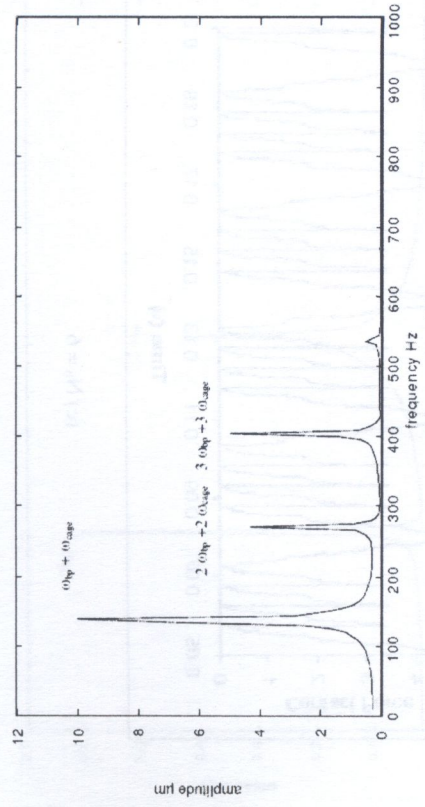
amplitude µm
frequency Hz

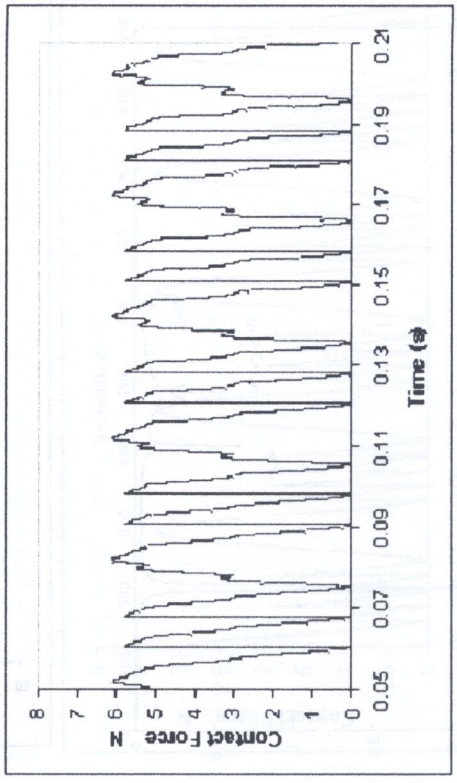
Contact Force N
Time (s)

(a) $N_b = 4$

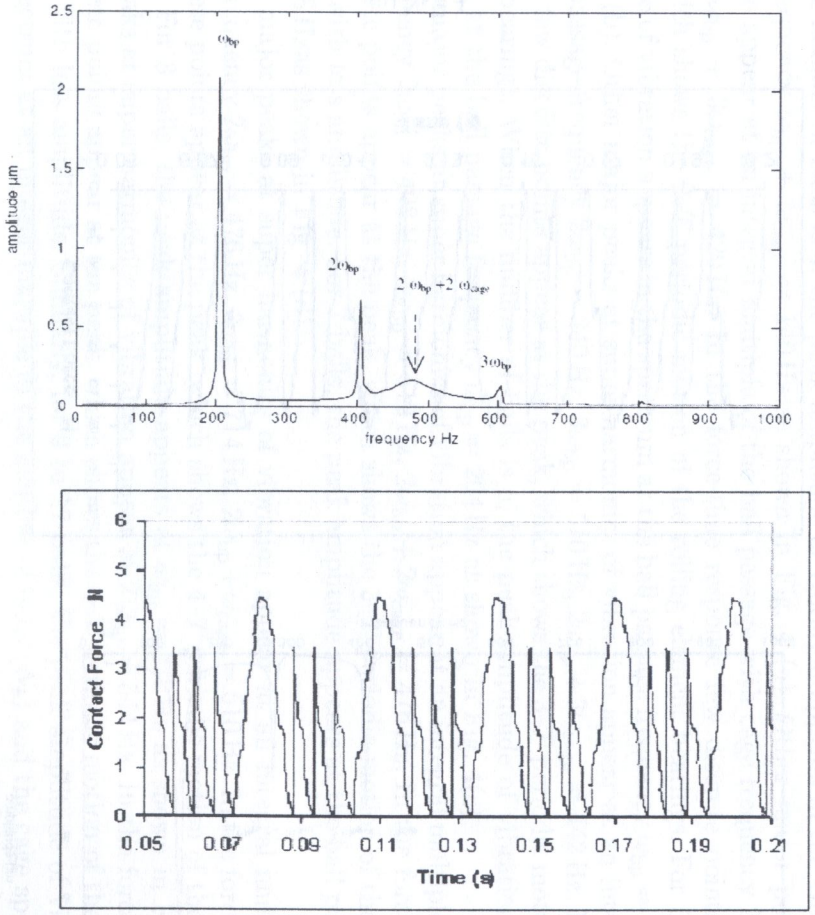
amplitude µm
frequency Hz
ω_{bp}
$2\omega_{bp}$
$2\omega_{bp}+2\omega_{cage}$
$3\omega_{bp}$
Contact Force N
Time (s)

(c) $N_b = 6$

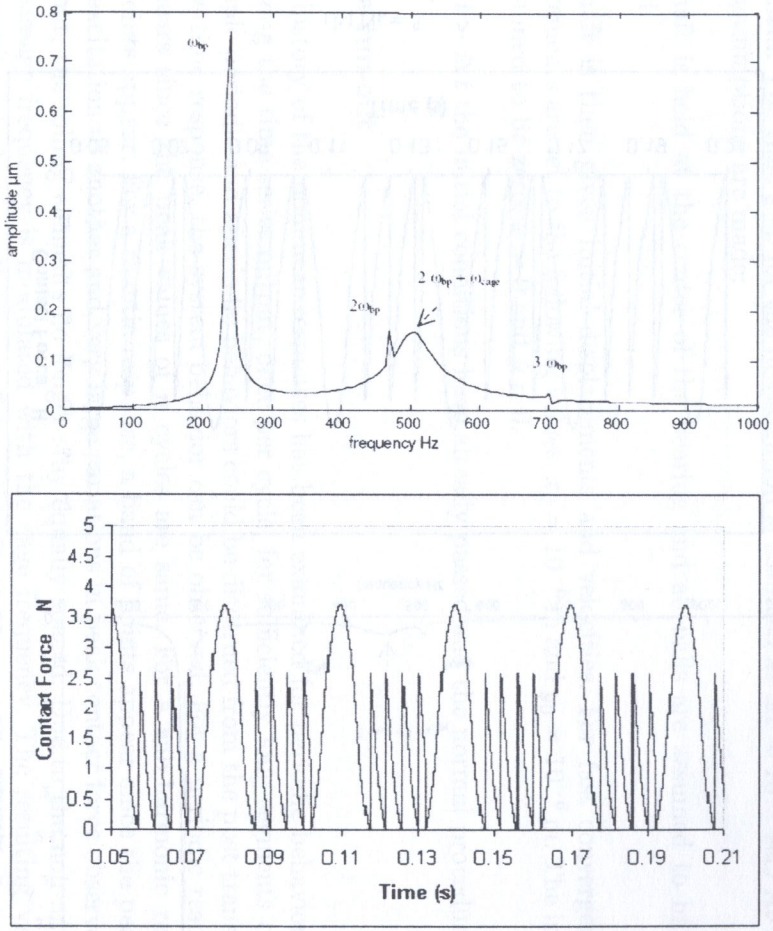
amplitude µm
frequency Hz
ω_{bp}
$2\omega_{bp}$
$2\omega_{bp}+\omega_{cage}$
$3\omega_{bp}$
Contact Force N
Time (s)

(d) $N_b = 7$

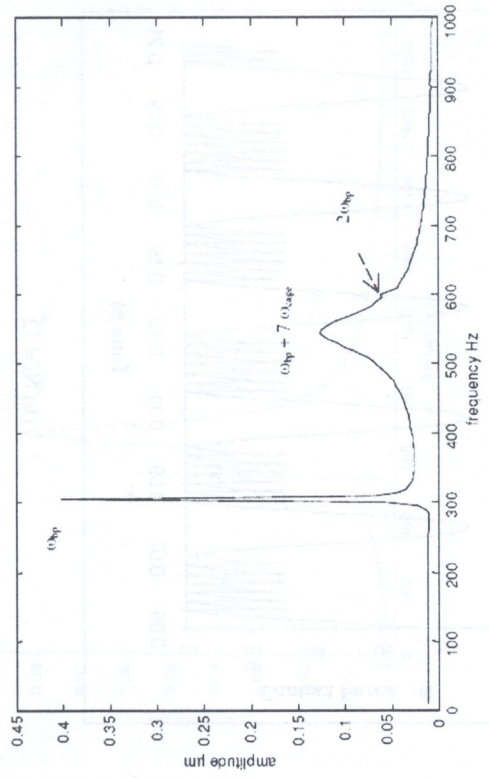
amplitude µm
frequency Hz
ω_{bp}
$\omega_{bp} + 7\,\omega_{cage}$
$2\omega_{bp}$

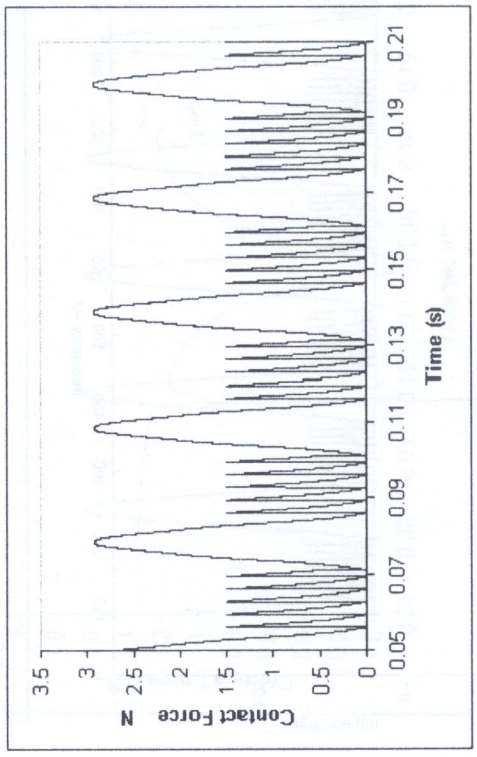
Contact Force N
Time (s)

(f) $N_b = 9$

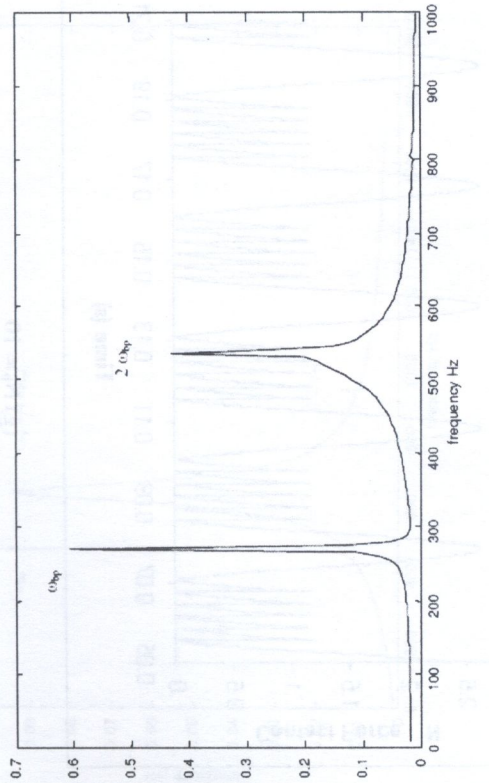
amplitude µm
frequency Hz
ω_{bp}
$2\,\omega_{bp}$

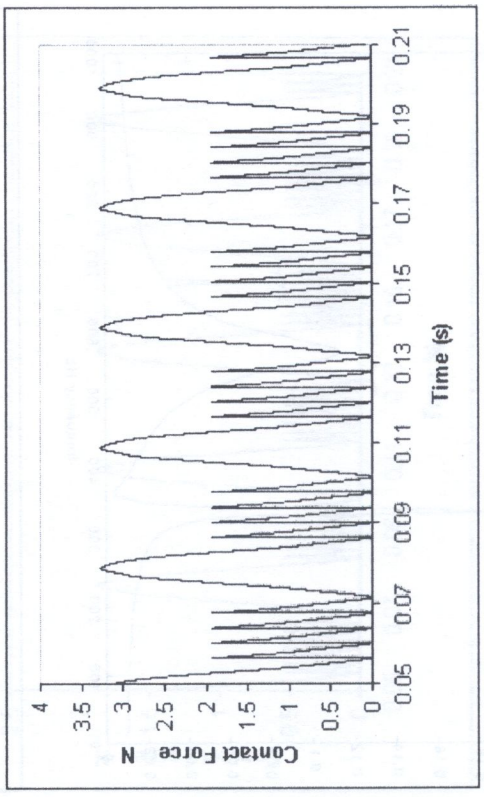
Contact Force N
Time (s)

(e) $N_b = 8$

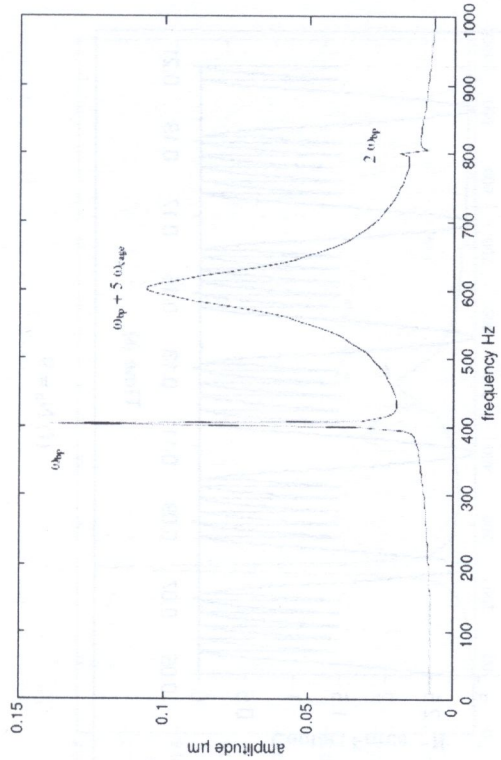
amplitude µm
frequency Hz
ω_{bp}
$\omega_{bp} + 5\ \omega_{cage}$
$2\ \omega_{bp}$

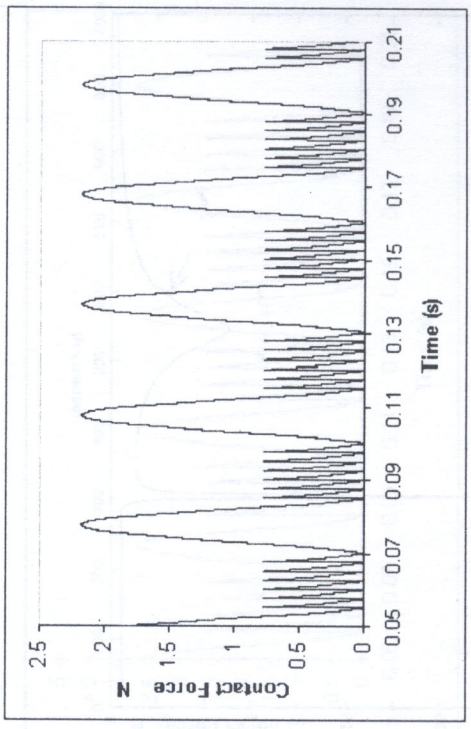
Contact Force N
Time (s)

(h) $N_b = 12$

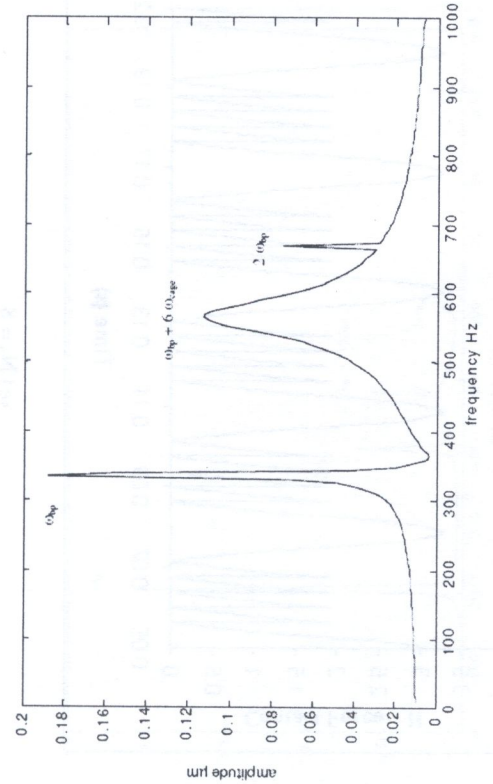
amplitude µm
frequency Hz
ω_{bp}
$\omega_{bp} + 6\ \omega_{cage}$
$2\ \omega_{bp}$

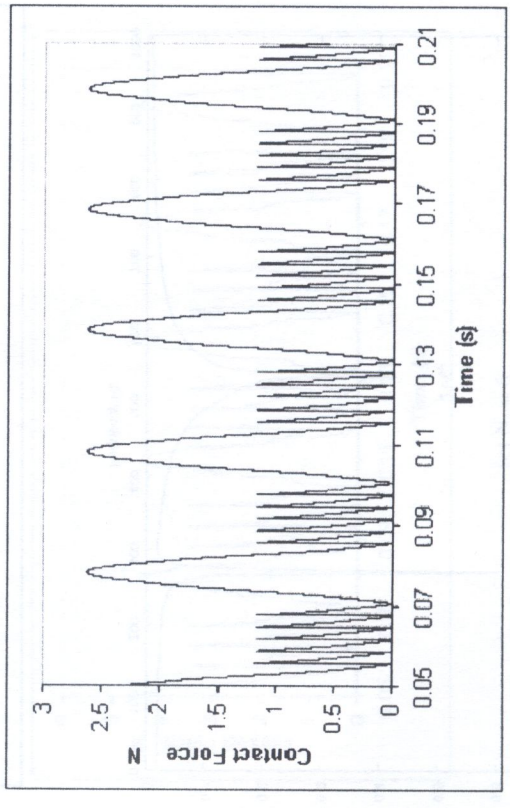
Contact Force N
Time (s)

(g) $N_b = 10$

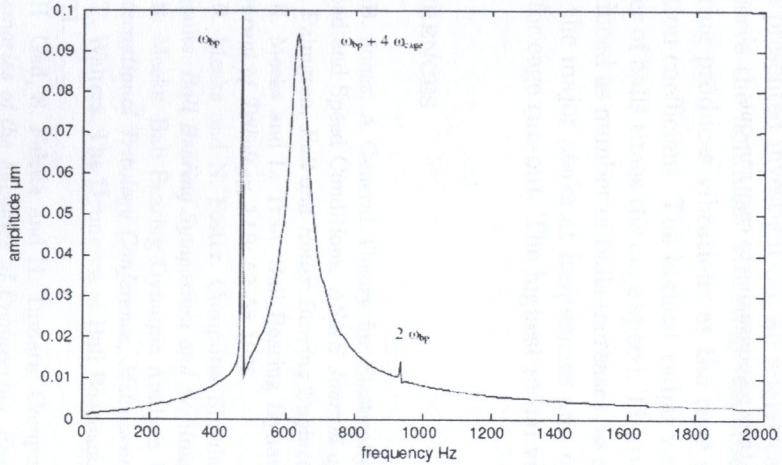
amplitude µm
frequency Hz
ω_{bp}
$\omega_{bp} + 4\,\omega_{cage}$
$2\,\omega_{bp}$

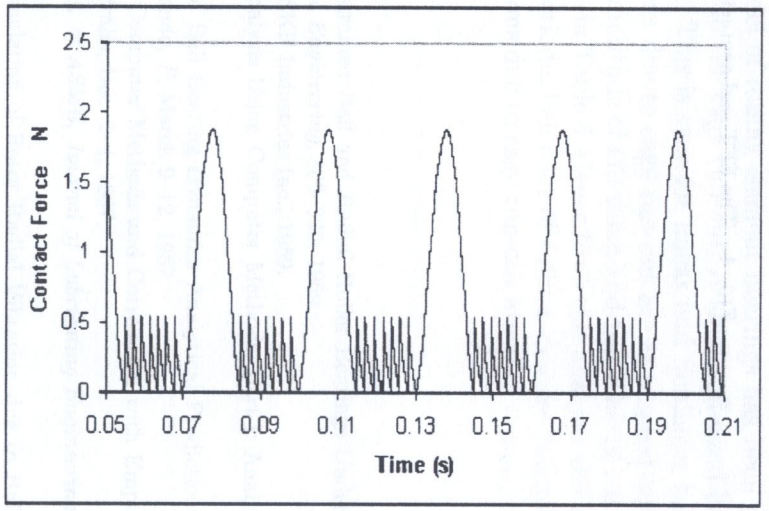
Contact Force N
Time (s)

(i) $N_b = 14$

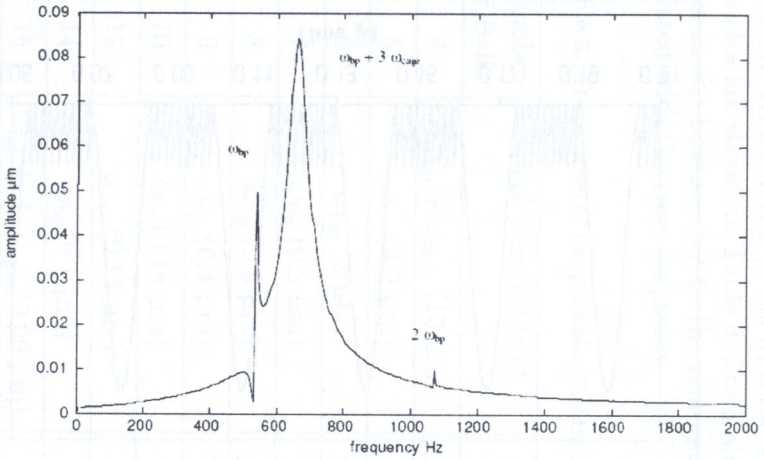
amplitude µm
frequency Hz
$\omega_{bp} + 3\,\omega_{cage}$
ω_{bp}
$2\,\omega_{bp}$

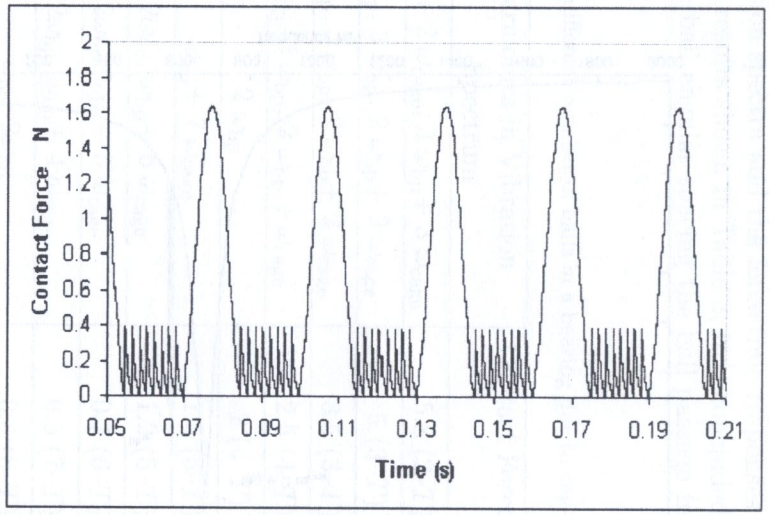
Contact Force N
Time (s)

(j) $N_b = 16$

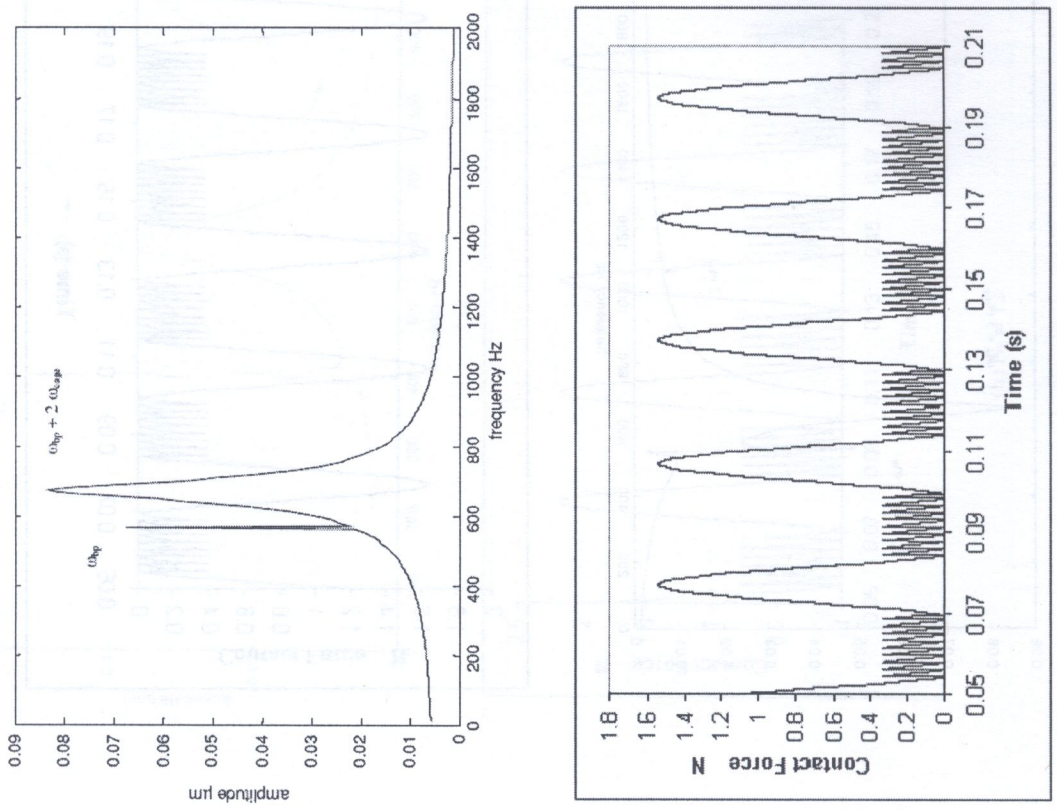

(k) $N_b = 17$

FIG. 4. The FFT and contact force-time response due to cage run-out

the $n-T$ periodic motion appear in the force-time response, which is shown in Figs. 4 (f) to (k), respectively. Other major peaks in these vibration spectra and the force-time responses with their amplitudes are shown in Table 3. From all the results shown in Table 3, it is concluded that cage run-out in the bearing due to the non-uniform ball angular spacing the ball passage frequency is modulated with the cage frequency.

Table 3. Frequencies of the possible vibrations for different number of balls in a bearing due to cage run-out

Number of Balls	Peak amplitude at	Harmonics in Vibration Spectrum	Contact Force (N)
4	$\omega_{bp} + \omega_{cage}$ (10 μm)	$2\omega_{bp}+ 2\ \omega_{cage}$, $3\ \omega_{bp}+ 3\ \omega_{cage}$	5.8 (2–T)
5	ω_{bp} (4.2 μm)	$2\ \omega_{bp}$, $3\ \omega_{bp}$, $2\ \omega_{bp}+ 3\ \omega_{cage}$	5 (3–T)
6	ω_{bp} (2 μm)	$2\ \omega_{bp}$, $3\ \omega_{bp}$, $2\ \omega_{bp}+ 2\ \omega_{cage}$	3.5 (3–T)
7	ω_{bp} (0.8 μm)	$2\ \omega_{bp}$, $3\ \omega_{bp}$, $2\ \omega_{bp} + \omega_{cage}$	2.5 (4–T)
8	ω_{bp} (0.6 μm)	$2\ \omega_{bp}$	2 (4–T)
9	ω_{bp} (0.4 μm)	$\omega_{bp}+ 7\ \omega_{cage}$	1.5 (5–T)
10	ω_{bp}(0.18 μm)	$2\omega_{bp}$, $\omega_{bp}+ 6\ \omega_{cage}$	1.2 (5–T)
12	ω_{bp} (0.14 μm)	$2\omega_{bp}$, $\omega_{bp}+ 5\ \omega_{cage}$	0.7 (6–T)
14	ω_{bp}(0.1 μm)	$2\omega_{bp}$, $\omega_{bp}+ 4\ \omega_{cage}$	0.5 (7–T)
16	$\omega_{bp} + 3\ \omega_{cage}$ (0.09 μm)	ω_{bp}, $2\omega_{bp}$	0.4 (8–T)
17	$\omega_{bp} + 2\ \omega_{cage}$ (0.09 μm)	ω_{bp}	0.3 (9–T)

4. Conclusion

In the presented investigation, an analytical model of rolling element bearings has been developed to observe the nonlinear vibration response due to the cage run-out. A single off-sized ball within a bearing produces vibrations at the cage speed. This is true for linear and nonlinear ball to race deflection coefficient. The highest radial vibrations due to cage run-out are at a speed equal to the number of balls times the cage speed. The peak amplitude of vibration and the value of contact force are reduced as number of balls increases, as shown in Table 3. Hence from this analysis the prediction about the major peaks at frequencies and n–T periodic behavior of rolling element bearings can be made for cage run-out. The highest radial vibrations due to cage run-out are at $\omega = a\omega_{bp} \pm b\omega_{cage}$.

References

[1] A.B. Jones. A General Theory for Elastically Constrained Ball and Radial Roller Bearings Under Arbitrary Load and Speed Conditions. *ASME Journal of Basic Engineering*, 309–320, 1959.

[2] A. Palmgren. *Ball and Roller Bearing Engineering.* SKF Industries Inc., 1959.

[3] C.R. Meeks and L. Tran. Ball Bearing Dynamic Analysis Using Computer Methods, Part-I: Analysis. *ASME Journal of Tribology*, **118**: 52–58 1996.

[4] C.R. Meeks and N. Foster. Computer Simulation of Ball Bearing Dynamics Analytical Predictions and Test Results. *Ball Bearing Symposium and Seminar, Orlando, F*, March 9–12, 1987.

[5] C.R. Meeks. Ball Bearing Dynamic Analysis Using Computer Methods and Correlation with Empirical Data. *International Tribology Conference, Melbourne, Australia*, Dec. 2–4, 1987.

[6] C.T. Walters. The Dynamics of Ball Bearings. *Trans. of ASME, Journal of Lubricating Engineering*, **93**: 1–10, 1971.

[7] E.H. Gad, S. Fukata and H. Tumara. Computer Simulation of Rotor Radial Vibration due to Ball Bearings. *Memories of the Faculties of Engineering, Kyushu universities*, **44**: 83–111, 1984 (a).

[8] E. Kramer. *Dynamics of rotors and foundations* New York: Springer, 1993.

[9] H. Rahnejat and R. Gohar. The Vibrations of Radial Ball Bearings. *Proceedings of the Institution of Mechanical Engineers*, **199** (C3): 181–193, 1985.

[10] J.W. Kennel and S.S. Bupara. A Simplified Model of Cage Motion in Angular Contact Bearings Operating in the EHD Lubricating Regime. *ASME Journal of Lubricating Technology*, **101**: 395–401, 1978.

[11] K. Bathe and E. Wilson, *Numerical Methods in Finite Element Analysis,* Prentice-Hall Englewood Cliffs, NJ, 1976.

[12] N. Aktürk, M. Uneeb and R. Gohar. The Effects of Number of Balls and Preload on Vibrations Associated Ball Bearings. *ASME Journal of Tribology*, **119**: 747–753, 1997.

[13] P. Eschmann, *Ball and Roller Bearings- Theory, Design and Application.* Willey, New York, 1985.

[14] P.K. Gupta. *Advanced Dynamics of Rolling Element Bearings,* Springer Verlag, 1984.

[15] P.K. Gupta. The Dynamics of Rolling Element Bearings, Part-III: Ball Bearing Analysis. *Trans. of ASME*, **101**: 51–70, 1979.

[16] S.P. Harsha, K. Sandeep and R. Prakash. Effects of Preload and Number of Balls on Nonlinear Dynamic Behaviors of Ball Bearing System. *International Journal of Nonlinear Sciences and Numerical Simulation*, **4**(3): 265–278, 2003.

[17] S.P. Harsha, K. Sandeep and R. Prakash. Nonlinear Dynamic Behaviors of Rolling Element Bearings Due to Surface Waviness. *Journal of Sound and Vibration*, **272**(3–5): 557–580, 2004.

[18] S.P. Harsha, K. Sandeep and R. Prakash. The Effect of Speed of Balanced Rotor on Nonlinear Vibrations Associated With Ball Bearings. *International Journal of Mechanical Sciences*, **47**(4): 225–240, 2003.

[19] T.A. Harris. *Rolling Bearing Analysis.* Willey, New York, 1991.